数理解析研究所講究録
第2058巻 2017年 148-161

Turbulence in quantum hydrodynamics

Michikazu Kobayashi
Department Physics, Kyoto University

By numerically solving the Gross-Piteavskii equation with the energy injection and dissipation, we study quantum turbulence comprised of quantized vortices with discrete circulations. We consider two opposite cases of fully developed quantum turbulence with strong energy injections and transition from quantum turbulence with vortices to vortex-free state with weak energy injections. With strong energy injections, the obtained energy spectrum for fully developed quantum turbulence has two scaling regions separated by the scale of the mean inter-vortex distance. In scales larger than the mean inter-vortex distance, the energy spectrum shows the well-known Kolmogorov law with the exponent $-5/3$. In scales smaller than the mean inter-vortex distance, on the other hands, the exponent of the energy spectrum changes to $-7/5$ suggesting that quantum turbulence is dominated by the Kelvin-wave cascade process of a single vortex line. With weak energy injections, the vortex-line density monotonically decreases with decreasing the strength of the energy injection and vanishes at the certain value of the energy injection. Close to the transition point, the vortex-line density can be regarded as the order parameter of the transition, showing its power-law behavior with the critical exponent 0.81. This value of the critical exponent is consistent with that for the $(3+1)$-dimensional directed percolation, which suggests the same underlying physics for two transitions of the directed percolation and quantum turbulence.

1 Introduction

Quantum fluid realized in supefluid helium and atomic Bose-Einstein condensates near the absolute zero temperature has become one great topic in various field of physics such as low temperature physics, fluid physics, quantum physics, statistical physics, cosmology, and so on [1]. The most important hydrodynamic property of quantum fluid is that any kind of flow is either inviscid and irrotational or carried by quantized vortices with a fixed circulation. The above feature of quantum fluid originates from the spontaneous breaking of the $U(1)$ symmetry for the phase shift of the order parameter and the flow is given as the gradient of the phase of the order parameter. Quantized vortices in quantum fluid are realized as topological line defects as a result of the $U(1)$ symmetry breaking.

Under the mean-field approximation and assuming the short-ranged inter-particle interaction, we can write down the equation for the time evolution of the order parameter known as the Gross-Pitaevskii (GP) equation which has the form of the Non-linear Schrödinger equation having the third order nonliearity. The GP equation satisfies the hydrodynamic property of quantum fluid and enables us to study the *quantum hydrodynamics*.

One of the most active topics in the quantum hydrodynamics is quantum turbulence realized in quantum fluid. As well as conventional turbulence with a large number of eddies having various

scales described by the Navier-Stokes equation, quantum turbulence is realized as temporary and spatially complicated structures of quantized vortices. The important differences between quantized vortices in quantum turbulence and eddies in conventional turbulence are (i) circulations of quantized vortices are concentrated in their cores and (ii) possible circulations are discrete. In this work, we numerically study the GP equation and consider two topics of quantum turbulence in which the above characteristics of quantum vortices plays an important role: (i) the kinetic energy spectrum of the statistically steady state of fully developed quantum turbulence and (ii) transition from turbulent to vortex-free states.

This proceeding is organized as follows. In Sec. 2, we briefly show how to derive the GP equation from the microscopic many-body Schrödinger equation with the mean-field approximation and the short-ranged inter-particle interaction potential [2]. The fundamental hydrodynamic property of the GP equation is also reviewed. In Secs. 3 and 4, we show our results about the energy spectrum of fully developed quantum turbulence (in Sec. 3) and transition from turbulent to vortex-free states (in Sec. 4). Section 5 provides the summary and concluding remarks.

2 GP equation and quantum hydrodynamics

2.1 Bose-Einstein condensation and GP equation

We start from the many-body Schrödinger equation with N-particle bosons with the mass M in 3-dimensional space:

$$\begin{aligned} i\hbar\frac{\partial}{\partial t}\Psi(\boldsymbol{x}_1,\cdots,\boldsymbol{x}_N,t) &= \left\{-\sum_{i=1}^{N}\frac{\hbar^2}{2M}\Delta_i+\frac{1}{2}\sum_{i\neq j}V(\boldsymbol{x}_i-\boldsymbol{x}_j)\right\}\Psi(\boldsymbol{x}_1,\cdots,\boldsymbol{x}_N,t) \\ &\equiv H_N\Psi(\boldsymbol{x}_1,\cdots,\boldsymbol{x}_N,t), \end{aligned} \tag{1}$$

where $\Psi(\boldsymbol{x}_1,\cdots,\boldsymbol{x}_N)$ is the N-particle wave function satisfying

$$\Psi(\boldsymbol{x}_1,\cdots,\boldsymbol{x}_i,\cdots,\boldsymbol{x}_j,\cdots,\boldsymbol{x}_N)=\Psi(\boldsymbol{x}_1,\cdots,\boldsymbol{x}_j,\cdots,\boldsymbol{x}_i,\cdots,\boldsymbol{x}_N), \tag{2}$$

for bosons. $V(\boldsymbol{x}_i-\boldsymbol{x}_j)$ is the two-body inter-particle interaction potential. In this proceeding, we do not consider the external 1-body potential such as a harmonic trap, magnetic and electric fields.

We define the following density matrix:

$$\rho^{(2)}(\boldsymbol{x},\boldsymbol{y},t)\equiv\int d^3x_2\cdots\int d^3x_N\,\Psi^*(\boldsymbol{x},\boldsymbol{x}_2,\cdots,\boldsymbol{x}_N,t)\Psi(\boldsymbol{y},\boldsymbol{x}_2,\cdots,\boldsymbol{x}_N,t). \tag{3}$$

With taking $\boldsymbol{y}\to\boldsymbol{x}$, the density matrix gives the density $\rho(\boldsymbol{x},t)$. In the limit of $|\boldsymbol{x}-\boldsymbol{y}|\to\infty$, we sometimes encounter the condition

$$\rho^{(2)}(\boldsymbol{x},\boldsymbol{y},t)\xrightarrow{|\boldsymbol{x}-\boldsymbol{y}|\to\infty}\psi^*(\boldsymbol{x},t)\psi(\boldsymbol{y},t)\neq 0. \tag{4}$$

If Eq. (4) is satisfied for the time-independent ground state Ψ_{G0} for Eq. (1) with the lowest eigenenergy E_{G} of the Hamiltonian H_N defined as

$$\begin{aligned} &E_{\mathrm{G}}\Psi_{\mathrm{G0}}(\boldsymbol{x}_1,\cdots,\boldsymbol{x}_N)=H_N\Psi_{\mathrm{G0}}(\boldsymbol{x}_1,\cdots,\boldsymbol{x}_N), \\ &\Psi_{\mathrm{G}}(\boldsymbol{x}_1,\cdots,\boldsymbol{x}_N,t)=e^{-iE_{\mathrm{G}}/\hbar}\Psi_{\mathrm{G0}}(\boldsymbol{x}_1,\cdots,\boldsymbol{x}_N), \end{aligned} \tag{5}$$

then, the system is defined as the Bose-Einstein condensation state. Equation (4) shows the spontaneous breaking of the $U(1)$ symmetry for the global phase shift of the order parameter $\psi(\boldsymbol{x})$. The condensate density is defined as $\rho_{\rm c} \equiv |\psi|^2 = |\lim_{|\boldsymbol{x}-\boldsymbol{y}|\to\infty} \rho^{(2)}|$. The condensate fraction

$$n_{\rm c} \equiv \frac{\rho_{\rm c}}{\rho} = \frac{\left|\lim_{|\boldsymbol{x}-\boldsymbol{y}|\to\infty} \rho^{(2)}(\boldsymbol{x},\boldsymbol{y})\right|}{\lim_{|\boldsymbol{x}-\boldsymbol{y}|\to 0} \rho^{(2)}(\boldsymbol{x},\boldsymbol{y})} \begin{cases} \sim 0.1, & \text{liquid } {}^4\text{He below 1 mK}, \\ \gtrsim 0.9, & \text{ultra-cold atomic gas}, \end{cases} \tag{6}$$

measures the intensity of the symmetry breaking. The exact definition of the Bose-Einstein condensation for the time-dependent state has not been constructed yet, we here regard the time-dependent Bose-Einstein condensation state when Eq. (4) is satisfied for the time-dependent wave function Ψ [3].

We next consider the following mean-field approximation:

$$\Psi(\boldsymbol{x}_1, \cdots, \boldsymbol{x}_N, t) \approx \prod_{i=1}^{N} \psi(\boldsymbol{x}_i, t). \tag{7}$$

Equation (7) consists of two kinds of approximations. The first one is that Ψ is approximated to be separated into single-particle state, and the second one is all separated single-particle state join the same state $\psi(\boldsymbol{x}, t)$. This approximation is rigorously satisfied only in the time-independent ground state for the ideal Bose gas with $V(\boldsymbol{x}_i - \boldsymbol{x}_j) = 0$ for arbitrary pairs of i and j. The approximation (7) gives the perfect Bose-Einstein condensation with the unit condensate fraction $n_{\rm c} = 1$ in Eq. (6), and the single-particle wave function ψ in Eq. (7) just becomes the order parameter defined in Eq. (4). The necessary condition for the validity of the mean-field approximation (7) is, therefore, that the condensate fraction $n_{\rm c}$ has to be close to unity. The density (or condensate density) is given by $\rho(\boldsymbol{x}, t) = |\psi(\boldsymbol{x}, t)|^2$.

Inserting Eq. (7) into the Schrödinger equation (1), we obtain the non-local GP equation

$$i\hbar\frac{\partial}{\partial t}\psi(\boldsymbol{x}, t) = \left\{-\frac{\hbar^2}{2M}\Delta + \int d^3y\, V(\boldsymbol{x}-\boldsymbol{y})|\psi(\boldsymbol{y}, t)|^2\right\}\psi(\boldsymbol{x}, t), \tag{8}$$

where we rewrite $\sqrt{N-1}\psi(\boldsymbol{x}, t)$ as $\psi(\boldsymbol{x}, t)$. We here replace the two-body inter-particle interaction potential $V(\boldsymbol{x}-\boldsymbol{y})$ as the short-ranged delta-functional form

$$V(\boldsymbol{x}-\boldsymbol{y}) \approx \frac{4\pi\hbar^2 a_s}{M}\delta(\boldsymbol{x}-\boldsymbol{y}) \equiv g\delta(\boldsymbol{x}-\boldsymbol{y}). \tag{9}$$

This assumption is valid when $V(r)$ rapidly goes to zero for $r \gg r_0$ with the effective length r_0, the density ρ is very low satisfying $\rho r_0^3 \ll 1$, and inter-particle scattering energy is so low that almost all inter-particle scattering are s-wave. The coefficient $4\pi\hbar^2 a_s/M$ can be obtained within the Born approximation, and a_s is the s-wave scattering length [4]. In this proceeding, we only consider the positive a_s. We shortly note that the analysis of the many-body Schrödinger equation (1) under the approximation (9) gives

$$1 - n_{\rm c} = \mathcal{O}\left(\sqrt{\rho a_s^3}\right), \tag{10}$$

for the time-independent ground state [5]. We therefore obtain the second necessary condition for the validity of the mean-field approximation (7) as $\rho a_s^3 \ll 1$. Inserting Eq. (9) into Eq. (8), we

finally obtain the GP equation

$$i\hbar\frac{\partial}{\partial t}\psi(\boldsymbol{x},t)=\left\{-\frac{\hbar^2}{2M}\Delta+g|\psi(\boldsymbol{x},t)|^2\right\}\psi(\boldsymbol{x},t). \tag{11}$$

In the following, we omit notations of the spatial and temporal dependence $(\boldsymbol{x},t)$ for all functions.

The GP equation (11) can be obtained from the following Hamilton equation:

$$i\hbar\frac{\partial\psi}{\partial t}=\frac{\delta\mathcal{E}}{\delta\psi^*},\quad \mathcal{E}=\int d^3x\left(\frac{\hbar^2}{2M}|\nabla\psi|^2+\frac{g}{2}\rho^2\right), \tag{12}$$

with the energy $\mathcal{E}$. We here introduce the Lagrange multiplier to satisfy that the uniform ground state with the density $\rho=\rho_0$ can be obtained by minimizing the energy as

$$\mathcal{E}-g\rho_0\mathcal{N}\equiv\mathcal{E}-g\rho_0\int d^3x\,\rho\to\mathcal{E}=\int d^3x\left\{\frac{\hbar^2}{2M}|\nabla\psi|^2+\frac{g}{2}(\rho-\rho_0)^2-g\rho_0^2\right\}. \tag{13}$$

The resulting GP equation becomes

$$i\hbar\frac{\partial\psi}{\partial t}=\left\{-\frac{\hbar^2}{2M}\Delta+g(\rho-\rho_0)\right\}\psi. \tag{14}$$

There is no qualitative difference between Eqs. (11) and (14) because Eq. (14) can be obtained by the phase shift of ψ as $\psi\to e^{-ig\rho_0 t/\hbar}\psi$ in Eq. (11).

2.2 Hydrodynamic property of GP equation

The time evolution of the density ρ becomes

$$\frac{\partial\rho}{\partial t}=-\nabla\cdot(\rho\boldsymbol{v}), \tag{15}$$

where $\boldsymbol{v}$ is defined as $\boldsymbol{v}=(\hbar/M)\nabla\arg[\psi]$. From this equation, $\boldsymbol{v}$ can be regarded as the fluid velocity, and its time evolution is

$$\frac{\partial\boldsymbol{v}}{\partial t}+\frac{1}{2}\nabla\boldsymbol{v}^2=-\frac{1}{M\rho}\nabla\left(\frac{g\rho^2}{2}\right)+\frac{\hbar^2}{2M^2}\nabla\left(\frac{\Delta\sqrt{\rho}}{\sqrt{\rho}}\right). \tag{16}$$

Equation (16) is the conventional Euler equation for the barotropic fluid with the pressure $g\rho^2/2$, when we ignore the second term of the right-hand side. This additional term which is absent from the Euler equation is known as the quantum pressure. The energy $\mathcal{E}$ in Eq. (13) is rewritten as

$$\mathcal{E}=\int d^3x\left\{\frac{M}{2}\rho\boldsymbol{v}^2+\frac{g}{2}(\rho-\rho_0)^2-g\rho_0^2+\frac{\hbar^2}{2M}|\nabla\sqrt{\rho}|^2\right\}. \tag{17}$$

The first three terms are conventional fluid energy and the last term is defined as the quantum energy originated from the quantum pressure in Eq. (16).

The outstanding difference between quantum hydrodynamics and classical one is that the fluid velocity $\boldsymbol{v}$ is irrotational everywhere except for the one-dimensional singular lines of the order parameter ψ. The order parameter ψ rapidly decreases in the scale of the healing length $\xi=\hbar/\sqrt{Mg\rho_0}$ close to the lines and vanishes on the lines, and the phase $\arg[\psi]$ changes by integer

multiple of 2π around the lines. These singular lines are known as quantized vortices, and the circulation for a closed loop $\mathcal{L}$ becomes

$$\oint_{\mathcal{L}} d\boldsymbol{l} \cdot \boldsymbol{v} = \frac{hn}{M}, \quad n \in \mathbb{Z}. \tag{18}$$

Only when quantized vortices pierce the loop $\mathcal{L}$, the integer n takes nonzero values as $n \neq 0$. Equation (18) implies that all rotational flow are carried by quantized vortices with discrete circulation hn/M. If we omit the quantum pressure term in Eq. (16), the quantum nature in hydrodynamics with discretized circulations disappears.

2.3 Generating statistically steady turbulent state

The original GP equation (14) conserves not only total number of particles $\mathcal{N}$ but also the energy $\mathcal{E}$, and cannot create statistically steady and non-equilibrium turbulent state because it has neither the energy injection in large scales nor the energy sink in small scales. We therefore modify the GP equation (14) to obtain statistically steady turbulence.

2.3.1 Energy sink in GP equation

We consider the Ginzburg-Landau (GL) equation

$$\hbar \frac{\partial}{\partial t}\psi = -\gamma \left\{ -\frac{\hbar^2}{2M}\Delta + g(\rho - \rho_0) \right\} \psi. \tag{19}$$

Although this equation is similar to the GP equation, it conserves neither the total number of particles $\mathcal{N}$ nor the energy $\mathcal{E}$, and the wave function ψ is attracted into the uniform ground state $\rho(\boldsymbol{x}, t \to \infty) \to \rho_0$ under the time evolution with losing the energy $\mathcal{E}$. Here $\gamma > 0$ is the dissipation constant. We combine the GP equation (14) and the GL equation (19) as

$$\hbar \frac{\partial}{\partial t}\psi = -(i + \gamma) \left\{ -\frac{\hbar^2}{2M}\Delta + g(\rho - \rho_0) \right\} \psi. \tag{20}$$

As well as the GL equation, ψ is attracted in the uniform ground state. This equation can be rewritten as

$$\frac{\partial \rho}{\partial t} + \nabla \cdot (\rho \boldsymbol{v}) = \frac{2\gamma}{\hbar} \left\{ \frac{\hbar^2}{2M}\sqrt{\rho}\Delta\sqrt{\rho} - \frac{M}{2}\rho \boldsymbol{v}^2 - g\rho(\rho - \rho_0) \right\}, \tag{21a}$$

$$\frac{\partial \boldsymbol{v}}{\partial t} + \frac{1}{2}\nabla \boldsymbol{v}^2 = -\frac{1}{\rho}\nabla\left(\frac{g\rho^2}{2M}\right) + \frac{\hbar^2}{2M^2}\nabla\left(\frac{\Delta\sqrt{\rho}}{\sqrt{\rho}}\right) + \frac{\gamma\hbar}{2M}\nabla\left\{\frac{\nabla \cdot (\rho \boldsymbol{v})}{\rho}\right\}. \tag{21b}$$

The last term of the right-hand side of Eq. (21b) works as the diffusion with the effective kinematic viscosity $\nu_{\text{eff}} \equiv \gamma\hbar/(2M)$. Equation (21a) shows that the total number of particles $\mathcal{N}$ is not conserved either. To avoid this, we introduce the time dependence of ρ_0 as $\rho_0 = \rho_0(t)$ to satisfy

$$\int d^3x \left\{ \frac{\hbar^2}{2M}\sqrt{\rho}\Delta\sqrt{\rho} - \frac{M}{2}\rho \boldsymbol{v}^2 - g\rho(\rho - \rho_0) \right\} = 0. \tag{22}$$

Introducing the dissipation term γ can be phenomenologically understood as the interaction between the condensate and its fluctuations by the thermal environment and the discrepancy from the mean-field approximation.

2.4 Energy injection in GP equation

We here introduce the energy injection by adding the external current $\boldsymbol{u}$ as

$$i\hbar\frac{\partial\psi}{\partial t} = \left\{-\frac{\hbar^2}{2M}\Delta + i\hbar\nabla\cdot\boldsymbol{u} + g(\rho-\rho_0)\right\}\psi. \tag{23}$$

In the hydrodynamic form, Eq. (23) is rewritten as

$$\frac{\partial\rho}{\partial t} + \boldsymbol{u}\cdot\nabla\rho + \nabla\cdot(\rho\boldsymbol{v}) = 0, \tag{24}$$

$$\frac{\partial\boldsymbol{v}}{\partial t} - \nabla(\boldsymbol{v}\cdot\boldsymbol{u}) + \frac{1}{2}\nabla\boldsymbol{v}^2 = -\frac{1}{\rho}\nabla\left(\frac{g\rho^2}{2M}\right) + \frac{\hbar^2}{2M^2}\nabla\left(\frac{\Delta\sqrt{\rho}}{\sqrt{\rho}}\right). \tag{25}$$

Combining Eqs. (20) and (23), we obtain

$$\begin{aligned}
&\hbar\frac{\partial\psi}{\partial t} = -i\left\{-\frac{\hbar^2}{2M}\Delta^2 + i\hbar\boldsymbol{u}\cdot\nabla + g(\rho-\rho_0)\right\}\psi - \gamma\left\{-\frac{\hbar^2}{2M}\Delta + g(\rho-\rho_0)\right\}\psi, \\
\Leftrightarrow\ &\begin{cases}
\dfrac{\partial\rho}{\partial t} + \boldsymbol{u}\cdot\nabla\rho + \nabla\cdot(\rho\boldsymbol{v}) = \dfrac{2\gamma}{\hbar}\left\{\dfrac{\hbar^2}{2M}\sqrt{\rho}\Delta\sqrt{\rho} - \dfrac{M}{2}\rho\boldsymbol{v}^2 - g\rho(\rho-\rho_0)\right\}, \\
\dfrac{\partial\boldsymbol{v}}{\partial t} - \nabla(\boldsymbol{u}\cdot\boldsymbol{v}) + \dfrac{1}{2}\nabla\boldsymbol{v}^2 = -\dfrac{1}{\rho}\nabla\left(\dfrac{g\rho^2}{2M}\right) + \dfrac{\hbar^2}{2M^2}\nabla\left(\dfrac{\Delta\sqrt{\rho}}{\sqrt{\rho}}\right) + \nu_{\text{eff}}\nabla\left\{\dfrac{\nabla\cdot(\rho\boldsymbol{v})}{\rho}\right\}.
\end{cases}
\end{aligned} \tag{26}$$

We solve Eq. (26) under the condition (22) for the conservation of the total number of particles $\mathcal{N}$. With both the energy injection and the sink, we can obtain the statistically steady and non-equilibrium state.

3 Energy spectrum of fully developed quantum turbulence

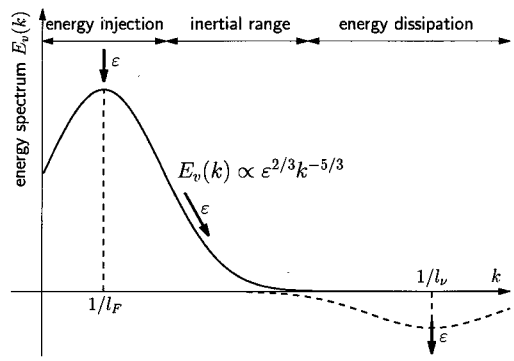

Figure 1: Wave-number dependence of the energy spectrum $E_v(k)$ (solid line) and the energy-dissipation rate $-2\nu k^2 E_v(k)$ (dashed line).

In this section, we report our result for the energy spectrum of fully developed quantum turbulence obtained by the numerical simulation of Eq. (26). Before discussing the energy spectrum

of quantum turbulence, we briefly review the energy spectrum of uniform, isotropic, and fully-developed classical turbulence obeying the incompressible Navier-Stokes equation. Figure 1 shows an outline of the kinetic-energy spectrum $E_v(k)$ defined as

$$E_v(k) = \frac{1}{L^3} \int \frac{k^2 d\Omega_k}{(2\pi)^3} \frac{1}{2} \left\langle |\tilde{\boldsymbol{v}}|^2 \right\rangle, \tag{27}$$

where $\tilde{\boldsymbol{v}}$ is the Fourier transformation of $\boldsymbol{v}$, $\int d\Omega_k$ is the solid-angle integration in the wave-number space at $k = |\boldsymbol{k}|$, and $\langle \cdots \rangle$ is the averaged over the time. There are only two scales l_F and l_ν. The scale l_F is that of the energy injection and usually the same order as the system size L. The scale l_ν is that where the energy dissipation by the kinematic viscosity ν becomes dominant, i.e., the wave-number dependent energy dissipation rate $2\nu k^2 E_v(k)$ becomes maximal at $k \approx 1/l_\nu$. The energy-dissipating scale l_ν is determined by the kinematic viscosity ν and the total energy dissipation rate ε defined by

$$\varepsilon = 2\nu \int dk\, k^2 E_v(k), \tag{28}$$

and it can be estimated as the Kolmogorov length scale $l_\nu \approx \sqrt[4]{\nu^3/\varepsilon}$. In the inertial range between two wave numbers $1/l_F \ll k \ll 1/l_\nu$, the viscosity has little effect on the energy spectrum, and $E_v(k)$ is believed to take the Kolmogorov's power-law form:

$$E(k) \propto \varepsilon^{2/3} k^{-5/3}, \tag{29}$$

independent of the kinematic viscosity ν.

We next report our numerical simulation of Eq. (26). The details of the simulation is as follows. We prepare a discretized periodic cubic box with 2048^3 grids. The spatial interval between two nearest grids is taken to be $\Delta x = 0.5\xi$, and the system size then becomes $L = 2048\Delta x = 1024\xi$. The dissipation constant is set to be $\gamma = 0.1$. To effectively create a fully developed turbulent state with many vortices, the incompressible external current $\boldsymbol{v}$ is more suitable than the compressible one. The external current $\boldsymbol{u}$ is fixed as follows. We first create smoothed random external current $\boldsymbol{u}_{\mathrm{r}}$ as

$$u_{\mathrm{r},i} = \frac{u_0}{8} \sum_{n_x,n_y,n_z=\pm 1} \cos\left(\frac{2\pi \boldsymbol{n}\cdot\boldsymbol{x}}{L} + \theta_{i,\boldsymbol{n}} \right), \tag{30}$$

for $i = x, y, z$. Here $-\pi < \theta_{i,\boldsymbol{n}} \le \pi$ take uniformly random values. The external current $\boldsymbol{u}_{\mathrm{r}}$ is gradually changing in a length scale of the system size L, and can be decomposed into the compressible and incompressible parts by the Helmholtz decomposition. We adopt the incompressible part of $\boldsymbol{u}_{\mathrm{r}}$ as $\boldsymbol{u}$. We solve Eq. (26) with the pseudo-spectral method in space and the fourth-ordered Runge-Kutta method in time. Here, we define the kinetic-energy spectrum $E_v(k)$ as

$$\int dk\, E_v(k) = \frac{1}{\mathcal{N}} \int d^3x \frac{1}{2} \left\langle \rho \boldsymbol{v}^2 \right\rangle \;\Leftrightarrow\; E_v(k) = \frac{1}{\mathcal{N}} \int \frac{k^2 d\Omega_k}{(2\pi)^3} \frac{1}{2} \left\langle |F[\sqrt{\rho}\boldsymbol{v}]|^2 \right\rangle, \tag{31}$$

where $F[A]$ is the Fourier transformation of A.

Figure 2 show our numerical results. After a long time evolution of Eq. (26) starting from a arbitrary initial state such as a uniform state $\psi = \sqrt{\rho_0}$, we can obtain a statistically steady

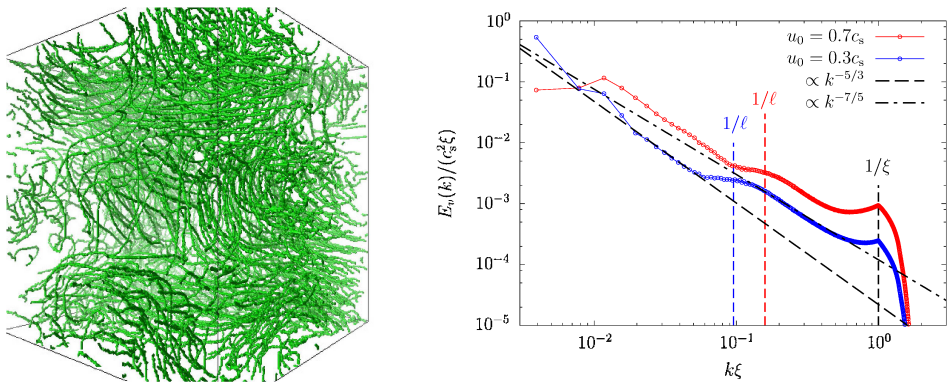

Figure 2: Left panel: Snapshot of a spatial vortex configuration for the statistically steady state of Eq. (26) with $u_0 = 0.7c_s$, where $c_s \equiv \sqrt{2g\rho_0/M}$ is the sound velocity. Right panel: Kinetic energy spectrum $E_v(k)$ defined in Eq. (31) with the amplitude of the external current $u_0 = 0.3c_s$ (blue curve) and $u_0 = 0.7c_s$ (red curve). Here, we take an ensemble average $\langle \cdots \rangle$ by taking the mean over 10 different external currents $\boldsymbol{u}$ with different $\theta_{i,j}$ and over 1000 different times for each external current $\boldsymbol{u}$. The wave number $1/\ell$ corresponding to the mean inter-vortex distance ℓ is also displayed for each u_0 with the corresponding color.

state independent of the initial states. The left panel shows one snapshot of a spatial vortex configuration. The right panel shows the obtained kinetic energy spectrum $E_v(k)$ with different amplitudes of the external current $u_0 = 0.3c_s$ and $0.7c_s$. In both cases, there are two power-law regions $E_v(k) \propto k^{-\eta_{\rm low,high}}$ separated by a bump structure, where two exponents $\eta_{\rm low,high}$ can be obtained by the fitting as $\eta_{\rm low} = 1.62(24)$ and $\eta_{\rm high} = 1.42(15)$ for lower and higher k regions respectively. The exponent $\eta_{\rm low}$ is very close to $5/3 \simeq 1.67$ and we expect that the Kolmogorov spectrum in Eq. (29) is also executed even in quantum turbulence and the quantum pressure in Eq. (16) has little effect on the property of quantum turbulence in large scales. This Kolmogorov-like spectrum does not continue to high wave-number region with the bump structure. The end of the Kolmogorov-like spectrum might be considered to be determined by the dissipation such that the Kolmogorov spectrum in classical turbulence does not continue at $k \approx 1/l_\nu$. We here estimate the effective Kolmogorov length $l_\gamma \equiv \sqrt[4]{\nu_{\rm eff}^3/\varepsilon}$ for Eq. (26). The total energy dissipation rate ε cannot be estimated from Eq. (28) because the kinetic energy may not only be dissipated with γ but also be transfered into the quantum energy defined in Eq. (17) through the quantum pressure. Instead of Eq. (28), we estimate the energy dissipation rate ε

$$\varepsilon \equiv -\left\langle \lim_{t\to 0} \frac{\partial \mathcal{E}}{\partial t} \right\rangle \simeq -\left\langle \frac{\varepsilon(t=\Delta t) - \varepsilon(t=0)}{\Delta t} \right\rangle, \tag{32}$$

after suddenly switching off the external current $\boldsymbol{u} = 0$ at $t = 0$. We then estimate the effective Kolmogorov length $l_\gamma \approx 0.8\xi$ and 0.5ξ for $u_0 = 0.3c_s$ and $0.7c_s$ respectively, and the wave-number $1/l_\gamma$ is much far from the position of the bump. We have also checked that the overall shape of $E_v(k)$ at $k < 1/\xi$ including the position of the bump and exponents $\eta_{\rm low,high}$ hardly change with the larger dissipation constant $\gamma = 0.3$. Therefore, we can conclude that introducing the dissipation

constant γ is not the origin of the end of the Kolmogorov-like spectrum with the appearance of the bump.

As another candidate of the end of the Kolmogorov-like spectrum, we expect that the quantum pressure becomes not negligible in this scale. Because the quantum pressure supports quantized vortices with the fixed circulation defined in Eq. (18), we can define mean inter-vortex distance ℓ as another scale specific to quantum turbulence. The mean inter-vortex distance ℓ can be defined as

$$\ell = \left\langle \sqrt{\frac{L^3}{L_{\rm vortex}}} \right\rangle, \tag{33}$$

where $L_{\rm vortex}$ is the total length of vortex lines in the system, and is estimated as $\ell \simeq 10.5$ and 6.25 for the external current $u_0 = 0.3$ and 0.7 respectively. In the right panel of Fig. 2, the positions of the wave number $1/\ell$ are shown and they agree with the positions of the bump. The end of the Kolmogorov-like spectrum and the appearance of the bump are, therefore, caused by the quantum pressure and quantized vortices with the fixed circulation.

In the higher wave-number region than the bump structure, quantum turbulence is dominated by single-vortex dynamics such as Kelvin waves excited along vortex lines. Assuming the process of the Kelvin-wave cascade in this wave-number region, several candidates for the exponent $\eta_{\rm high}$ have been theoretically predicted: $\eta_{\rm high} = 1$, 7/5, 5/3, and so on [6]. We here skip to review these theories, but note that our result supports the theory for $\eta_{\rm high} = 7/5 = 1.4$.

4 Transition from quantum turbulence to vortex-free state

In the previous section, we consider fully developed turbulence with strong energy injections far away from equilibrium state. In this section, we consider the opposite limit with weak energy injections. Under this condition, we can expect the transition or gradual change between quantum turbulence with quantized vortices and vortex-free state. By numerically solving Eq. (26), we study this boundary between them. Compared with classical turbulence, quantum turbulence has an advantage to study this research because we can directly estimate the strength of turbulence by total line length of vortices $L_{\rm vortex}$. Unlike the case of fully developed turbulence with the strong energy injection, we encounter a strong dependence on the spacial profile of the energy injection. We here consider the simple situation: the uniform external current $\boldsymbol{u} = \begin{pmatrix} u_0 & 0 & 0 \end{pmatrix}$ with the intensity u_0.

Equation (26) has the uniform and steady solution $\psi = \sqrt{\rho_0 - M\bar{v}^2/(2g)}e^{i(M/\hbar)\bar{v}(x+u_0t)}$ with the arbitrary velocity $\bar{v}$. The behavior of the non-uniform solution is, however, very difficult to be analytically treated. Especially, we are interested in whether the non-uniform solution is relaxed to the uniform solution or not, *i.e.*, whether quantum turbulence can survive or not under the uniform external current. To answer this question, we have performed the numerical simulations of Eq. (26) in the periodic cubic box with 1024×128^2 grids. The spatial interval is taken to be $\Delta x = 0.5\xi$, and the system size then becomes $L_x = 512\xi$ and $L_{y,z} = 64\xi$, where the external current $\boldsymbol{u}$ is applied along the x-direction. We start from the intensity of the external current as $u_0 = 1.6c_s$ and the initial state $\psi = \sqrt{\rho_0 - \hbar^2|\nabla\varphi|^2/(2Mg)}e^{i\varphi}$ with the smoothed random phase

$$\varphi = \frac{2\pi}{N} \sum_{|\boldsymbol{n}|\le 10, \boldsymbol{n}\neq 0} \cos\left(\frac{2\pi n_x x}{L_x} + \frac{2\pi n_y y}{L_y} + \frac{2\pi n_z z}{L_z} + \theta_{i,\boldsymbol{n}} \right), \tag{34}$$

where $c_s = \sqrt{2g\rho_0/M}$ is the sound velocity and N is the total number satisfying $|\boldsymbol{n}| \leq 10$, and perform the simulation of the GP equation (26) until the system reaches the statistically steady state. After calculating averaged physical values over the time, we continue the simulation with the slightly smaller external current $u_0 \to u_0 - 0.01c_s$ and obtain the statistically steady state. Repeating these processes, the system finally reaches the vortex-free state under the some external current which can be regarded as the critical external current from turbulent to vortex-free states.

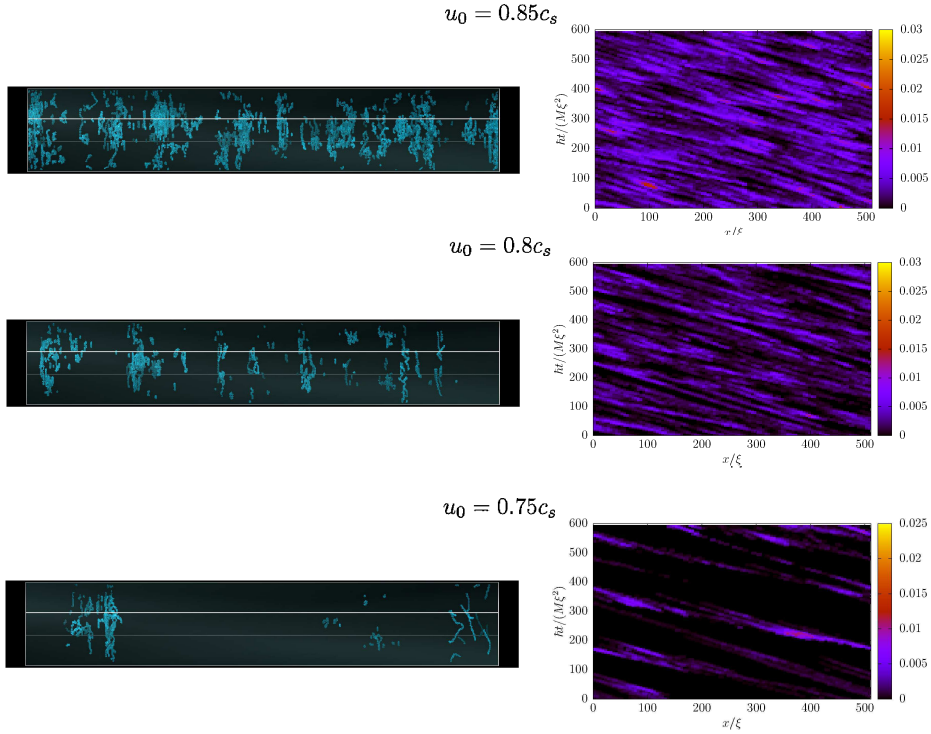

Figure 3: Right panels: Steady snapshots of spatial vortex configurations. Left panels: Dependences of integrated vortex-line density over the yz-plane on the coordinate x and the time t. Intensities of external currents u_0 are 0.85 (top panels), 0.8 (middle panels) and 0.75 (lower panels) respectively.

Left panels of Fig. 3 show snapshots of spatial vortex configurations with the intensities $u_0 =$ 0.75 (upper panel), 0.8 (middle panel), and 0.85 (lower panel). These three panels show that the system reaches non-uniform steady turbulent state with finite vortices. With decreasing the intensity u_0, vortices become non-uniformly more dilute showing a stripe structure, which indicates there exist repeating of locally turbulent and non-turbulent states. This feature can be clearly seen in right panels of Fig. 3 which show the dependence of integrated vortex-line density over yz plane on the coordinate x and t. We can see that several "turbulent clouds" having nonzero vortex

densities move in a constant velocity.

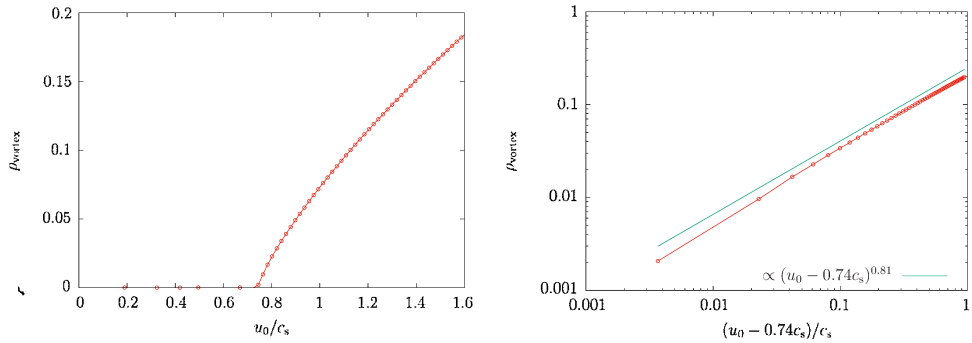

Figure 4: Left panel: Vortex-line density $\rho_{\rm vortex}$ as a function of the external current u_0 in a linear scale. Right panel : Vortex-line density $\rho_{\rm vortex}$ as a function of the external current $u_0 - 0.74c_{\rm s}$ in a log-log scale. Here the value $0.74c_{\rm s}$ is the critical external current at which the vortex-line density $\rho_{\rm vortex}$ vanishes.

Left panel in Fig. 4 shows the dependence of the vortex-line density $\rho_{\rm vortex}$ on the external current u_0. The vortex-line density $\rho_{\rm vortex}$ decreases with decreasing the external current u_0, and vanishes at $u_0 \equiv u_{0\rm c} \simeq 0.74c_{\rm s}$. We can expect the transition from quantum turbulence with vortices to vortex-free state occurs at the critical external current $u_{0\rm c}$. Right panel in Fig. 4 shows the same dependence as the left panel in log-log scale and the critical behavior of the vortex-line density as $\rho_{\rm vortex} \propto (u_0 - u_{0\rm c})^{\beta}$ with the critical exponent $\beta \simeq 0.81$. This result suggests that the obtained transition is non-equilibrium phase transition with regarding the vortex-line density $\rho_{\rm vortex}$ as the "order parameter" for quantum turbulence "phase". The value of the critical exponent $\beta \simeq 0.81$ is consistent with that for the $(3+1)$-dimensional directed percolation, suggesting that the obtained transition has the universality class for the directed percolation.

Here we briefly review the directed percolation [7]. In Fig. 5, we show examples of ordinary 2-dimensional bond isotropic percolation and $1+1$-dimensional bond directed percolation on a diagonal square lattice. In these models, bonds between adjacent sites of a square lattice are open with probability p and otherwise closed. As shown in the right panel of Fig. 5, there is a specific preferred direction in space. The bonds work as "valves" in a way that the spreading direction is fixed along the given direction, as indicated by the arrows. As in the case of isotropic percolation, directed percolation exhibits a continuous phase transition.

The phase transitions of both isotropic and directed percolations are characterized by an order parameter P_∞ which is defined as the probability that a randomly selected site generates an infinite cluster. In finite dimensions $2 \leq d < \infty$, there is a continuous phase transition separating $P_\infty = 0$ and $P_\infty > 0$ at some critical value $p = p_{\rm c}$ with $0 < p_{\rm c} < 1$. The critical threshold $p_{\rm c}$ for directed percolation is larger than that for isotropic percolation.

Numerical simulations of $(1+1)$-dimensional directed bond percolations with different probability p are illustrated in Fig. 6. In this figure, we show typical configurations starting from random conditions at the boundary along the preferred direction. Results changes significantly at the phase transition. For $p < p_{\rm c}$, the number of connecting bonds decreases exponentially along the preferred direction until the system reaches the state with no connecting bonds, whereas for

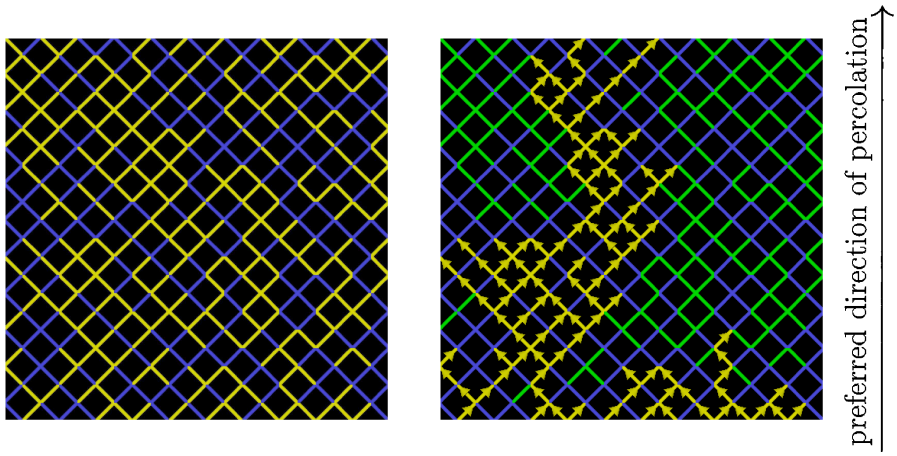

Figure 5: Examples of 2-dimensional bond isotropic percolation (left panel) and (1+1)-dimensional bond directed percolation (right panel) on a diagonal square lattice having the same configuration of open and closed bonds. In the left panel, open (closed) bonds are represented by yellow (blue) lines. In the right panel, the percolating direction is restricted to follow the sense of the arrows, leading to a directed cluster of connected sites. Some open bonds in the directed case are, therefore, cannot join in connected clusters as shown with green lines.

$p > p_c$ the number of connecting bonds saturates at some constant value. At the critical point the mean number of connecting bonds decays very slowly and the cluster of connecting bonds remind of fractal structures.

As well as the magnetization of the Ising model, the phase transitions of the isotropic percolation is characterized by universal scaling laws for the order parameter P_∞ as $P_\infty \propto (p - p_c)^\beta$ for $p > p_c$, where β is a universal exponent and depends on the spatial dimension. The same picture emerges in the directed percolation with the different critical exponent β from that for the isotropic percolation. For example, the exponent β takes $\beta \simeq 0.14$, 0.42, 0.66 for d-dimensional isotropic percolation with $d = 2$, 3, 4, and $\beta \simeq 0.28$, 0.58, 0.81 for $(d+1)$-dimensional directed percolation with $d = 1$, 2, 3.

We consider the relationship between the directed percolation and the transition from quantum turbulent to vortex-free states. For simplicity, we here assume that the space $\boldsymbol{x}$ and time t are discretized as $\boldsymbol{x_i}_{\in\mathbb{Z}^3}$ and $t_{j\in\mathbb{Z}}$, and all discretized spatial points can be separated into those with and without vortices. For example, we can imagine a spatial point with vortices as a spatial point in a turbulent cloud as shown in the lower-right panel of Fig. 4. We then define the binary function $s(\boldsymbol{x_i}, t_j)$ as

$$s(\boldsymbol{x_i}, t_j) = \begin{cases} 0, & \text{if there are vortices at } \boldsymbol{x_i}, \\ 1, & \text{if there is no vortex at } \boldsymbol{x_i}. \end{cases} \tag{35}$$

There is a large energy gap between states with and without vortices, vortices cannot be nucleated but spread due to the external uniform current or disappear due to the dissipation. We give intuitive

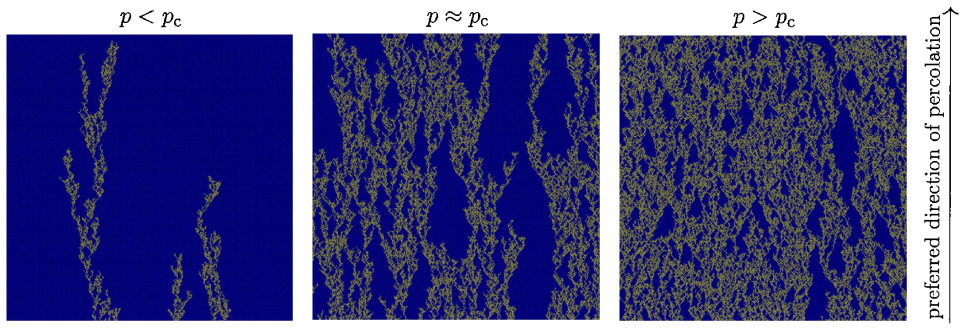

Figure 6: $(1+1)$-dimensional directed bond percolation starting from random conditions at the lower boundary.

interpretation of this condition as

$$s(\boldsymbol{x}_i, t_{j+1}) = \begin{cases} 1 & \text{if } \sum_k s(\boldsymbol{x}_i + \Delta\boldsymbol{x}_k, t_j) > 1 \text{ and } z(\boldsymbol{x}_i, t_j) < p, \\ 0 & \text{otherwise,} \end{cases} \tag{36}$$

where $\boldsymbol{x}_i + \Delta\boldsymbol{x}_k$ is the nearest neighboring spatial point to $\boldsymbol{x}_i$ and $\sum_k s(\boldsymbol{x}_i + \Delta\boldsymbol{x}_k, t_j) > 1$ means that there is at least one neighboring spatial point with vortices. $0 < z(\boldsymbol{x}_i, t_j) < 1$ is the uniformly distributed random number, and vortices can spread to the nearest sites with the probability p or disappear with the probability $1 - p$. Equation (36) is nothing but the condition for the $(3+1)$-dimensional directed percolation under the correspondence of the preferred direction to the time. If we regard the external current u_0 and the vortex-line density ρ_{vortex} as the probability p and the order parameter P_∞ with $u_0 \propto p$ and $\rho_{\text{vortex}} \propto P_\infty$, we obtain $\rho_{\text{vortex}} \propto (u_0 - u_{0c})^\beta$ which is consistent with our numerical result of the transition from quantum turbulent to vortex-free states giving the same critical exponent $\beta \simeq 0.81$. This result support that the underlying physics for the transition of the directed percolation and the transition from quantum turbulent to vortex-free states are same, and the intuitive discussion for quantum turbulence with using Eq. (36) is almost correct.

5 Summary

In this proceeding, we discuss two topics of quantum turbulence comprised of quantized vortices. The first topic is the energy spectrum of fully developed quantum turbulence under a strong energy injection. Being different from conventional turbulence described by the Navier-Stokes equation, there exists the mean inter-vortex distance ℓ as an additional scale in quantum turbulence, and there are two scaling regions of the energy spectrum separated by the wave number $\approx 1/\ell$. In the small wave-number region, the obtained energy spectrum is consistent with the well-known Kolmogorov law with the power $-5/3$. In the higher wave-number region, on the other hand, the obtained energy spectrum is characterized by the power $-7/5$ which is consistent with the theory for the Kelvin-wave cascade process of a single vortex line in quantum turbulence.

The second topic is the transition from quantum turbulence with vortices to vortex-free state under a weak energy injection. With decreasing the strength of the energy injection, we observe the

continuous transition from quantum turbulent to vortex-free states. Around the transition point, the vortex-line density can be regarded as the order parameter of the transition, showing its power-law behavior with the critical exponent. The obtained critical exponent is consistent with that for the $(3+1)$-dimensional directed percolation, which suggests that the underlying physics for the transition from quantum turbulent to vortex-free states is same as that for the transition of the $(3+1)$-dimensional directed percolation. This consistency between two models can be intuitively understood by considering the correspondence of the preferred dimension, probability p for open channels to be selected, and the order parameter P_∞ for the infinite percolating clusters in the directed percolation to the time, the external current u_0 and the vortex-line density ρ_{vortex} in quantum turbulence, respectively.

References

[1] K. H. Bennemann and J. B. Ketterson, *Nover Superfluids* (Oxford University Press, Oxford, England, 2013).

[2] A. J. Legget, *Quantum Liquids: Bose Condensation And Cooper Paring in Condensed-matter Systems* (Oxford University Press, Oxford, England, 2006).

[3] M. Ueda, *Fundamentals and New Frontiers of Bose-Einstein Condensation* (World Scientific, Singapore, 2010).

[4] C. J. Pethick and H. Smith, *Bose-Einstein Condensation in Dilute Gases* (Cambridge University Press, Cambridge, England, 2008).

[5] E. H. Lieb and R. Seiringer, Phys. Rev. Lett. **88**, 170409 (2002).

[6] W. F. Vinen and J. J. Niemela, J. Low Temp. Phys. **128**, 167 (2002); E. Kozik and B. Svistunov, Phys. Rev. Lett. **92**, 035301 (2004); L. Kodaurova, V. L'vov, A. Pomyalov, and I. Procaccia, Phys. Rev. B **90**, 094501 (2014).

[7] H. Hinrichsen, Adv. Phys. **49**, 815 (2000).